FEBS Letters 354 (1994) 37–40

FEBS 14672

A cryoelectron microscopy study of the interaction of the *Escherichia coli* F_1-ATPase with subunit *b* dimer

Stephan Wilkens[a], Stanley D. Dunn[b], Roderick A. Capaldi[a,*]

[a]*Institute of Molecular Biology, University of Oregon, Eugene, OR 97403, USA*
[b]*Department of Biochemistry, University of Western Ontario, London, Ont. N6A 5C1, Canada*

Received 31 August 1994

Abstract A complex between the *Escherichia coli* F_1-ATPase and a truncated form of the ECF_0–*b* subunit was formed and examined by cryoelectron microscopy in amorphous ice. Image analysis of single particles in the hexagonal projection revealed that the polar domain of the *b* subunit interacts with a β subunit different from the one which interacts with the ε subunit. The cavity in the enzyme, visible in the hexagonal projection, is not filled by the *b* polypeptide, therefore leaving enough room for extensive conformational changes of the γ and ε subunits within the native F_1F_0 complex.

Key words: Cryoelectron microscopy; F_1-ATPase; ATP synthase; *b* subunit

1. Introduction

An F_1F_0-type ATPase, found in the plasma membrane of bacteria, thylakoid membrane of chloroplasts and the inner membrane of mitochondria, functions to synthesize ATP in response to a light- or respiratory chain-driven proton gradient. This enzyme also works as an ATPase using the hydrolysis of ATP to establish a pH gradient for subsequent use in ion or substrate transport processes.

The simplest F_1F_0-type ATPases structurally are those from bacteria. The enzyme from *Escherichia coli* is made up of a total of eight different subunits; five in the F_1 part ($\alpha_3\beta_3\gamma\delta\varepsilon$) and three in the F_0 part (ab_2c_{10-12}) [1–3]. The interaction between F_1 and F_0 is through a narrow stalk of around 45 Å in length [4] which contains subunits of the F_1 part [5], and, in addition, appears to involve the *b* subunits of the F_0. The amino acid sequence of the *b* subunit includes an N-terminal, hydrophobic and membrane-spanning segment, followed by a long hydrophilic, highly charged, C-terminal region. Recently, one of us has genetically produced a truncated form of the *b* subunit from residues 25 to 156, called b_{sol}, that represents the polar C-terminal domain of this subunit [6]. The b_{sol} forms a stable dimer in solution which interacts with ECF_1, as shown by size-exclusion chromatography and competition experiments, in which b_{sol} blocked rebinding of F_1 to intact F_0.

Cryoelectron microscopy studies of ECF_1 and ECF_1F_0 have provided important information about the overall shape, the location of subunits, and the energy-dependent conformational changes that occur in these complexes [4,7–9]. Here, we have used cryoelectron microscopy to study the ECF_1–b_{sol} complex. The results show that b_{sol} superimposes in the hexagonal projection on a β subunit which is different from the β subunit that interacts with the ε subunit.

2. Materials and methods

The truncated, soluble form of the ECF_0–*b* subunit (b_{sol}) was isolated and characterized as described by Dunn [6]. ECF_1 was purified from an overproducing *E. coli* strain AN1460 according to Wise et al. [10] with the modifications described in Gogol et al. [11]. The Fab′ fragments derived from a monoclonal antibody against the α subunit used in this study are described in Aggeler et al. [12]. For cryoelectron microscopy, ECF_1 at a concentration of 0.04 mg/ml in 20 mM Tris-HCl, pH 7.2, 100 mM NaCl, 1 mM ethylenediaminetetraacetic acid (EDTA) and 2 mM ATP was mixed with a 5-fold molar excess each of b_{sol} and anti-α Fab′ fragments and incubated for 30 min at room temperature. The sample was then rapidly frozen for cryoelectron microscopy as described in Gogol et al. [7]. Cryoelectron microscopy and single particle image analysis was conducted as described in Wilkens and Capaldi [9]. For the image analysis, the SPIDER package of programs [13] was used.

3. Results

A complex between ECF_1 and b_{sol} was prepared according to Dunn [6], except that for cryoelectron microscopy a 5-fold excess of the b_{sol} dimer over F_1 was used to compensate for the moderate binding affinity of b_{sol} for F_1 (1–2 μM) [6].

Fig. 1 shows an electronmicrograph of the ECF_1–b_{sol} complex, embedded in a thin layer of amorphous ice. The molecules are additionally labeled with Fab′ fragments derived from a monoclonal antibody against the α subunit to ensure a uniform hexagonal orientation of the enzyme complexes in the thin ice layer. For single particle image analysis, a dataset of 603 molecular images was selected from two electron micrographs. The single images were first band pass filtered to remove high and low spatial frequencies, followed by an iterative alignment to the strong asymmetric features of the $ECF_1(\alpha I\ Fab')_3$ complex (see below) and finally treated by correspondence analysis and classification methods.

Fig. 2A shows the total average of the dataset after three rounds of alignment; Fig. 2B shows an average of 366 $ECF_1(\alpha I\ Fab')_3$ complexes, analysed the same way as the b_{sol}-labeled molecules. The major features of the averages in Fig. 2A and B are the three triangularly arranged α subunits, each labeled with an Fab′ fragment, the three β subunits, alternating with the α subunits, a central mass located nearest to one of the β subunits and a central cavity located next to a different β subunit.

Wilkens and Capaldi [9] have shown that the $ECF_1(\alpha I\ Fab')_3$ complex displays a strong asymmetry in the hexagonal projec-

*Corresponding author. Fax: (1) (503) 346-5891.

SSDI 0014-5793(94)01059-5

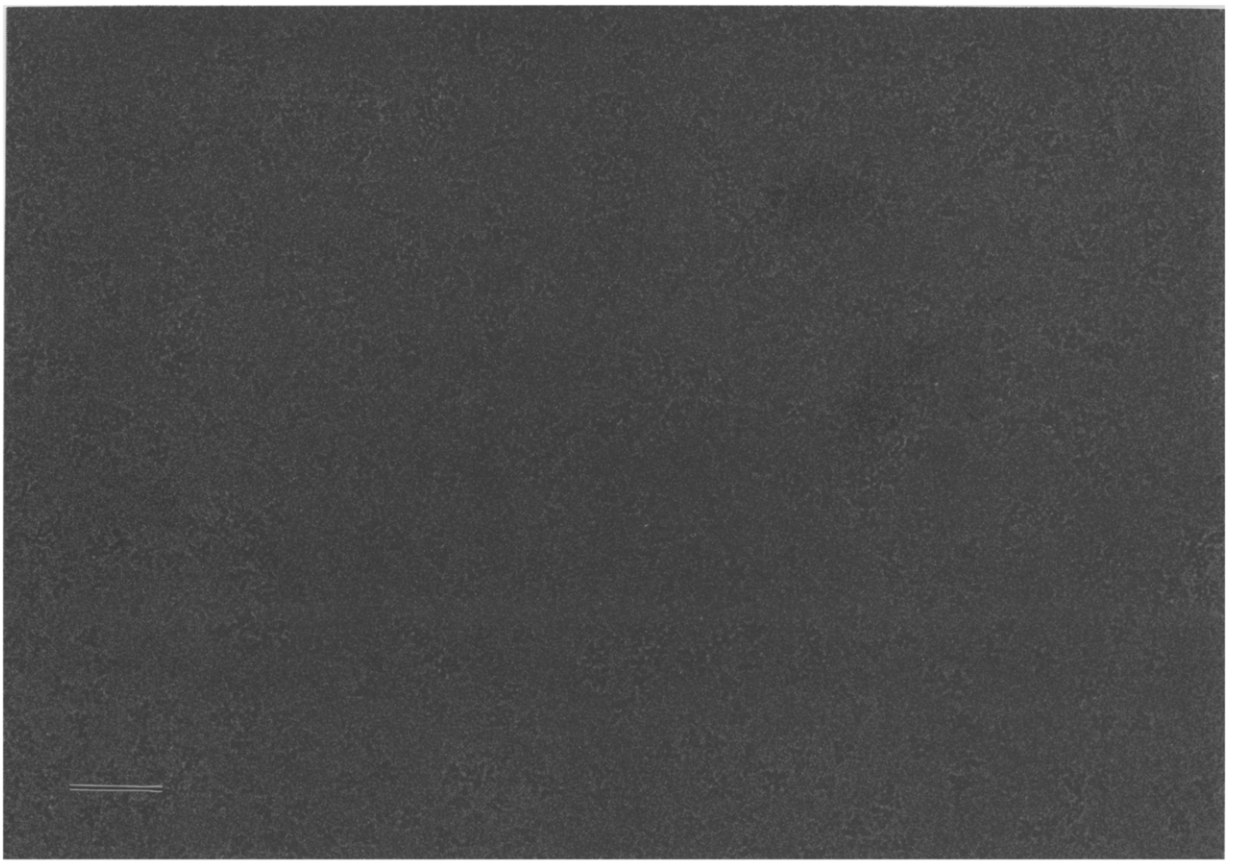

Fig. 1. Cryoelectron micrograph of the ECF_1–b_{sol} complex, additionally labeled with anti-α Fab′ fragments to ensure a uniform orientation of the molecules in the ice layer. Electron optical magnification ×60,000. Bar = 50 nm.

tion which manifests itself in the projection intensities of the β subunits, the distances between the β subunits and the location of the central cavity and the central mass. Due to this asymmetry of the complex, the three different β subunits could be distinguished and were called β1 (top), β2 (bottom left) and β3 (bottom right).

There is no obvious additional density visible in the molecule labeled with b_{sol} (Fig. 2A). However, careful examination of the average indicated a greater density of the bottom left β (β2) compared to the average of the unlabeled complex (Fig. 2B). This could be confirmed by subtracting the average shown in Fig. 2B from the average shown in Fig. 2A, creating the difference map shown in Fig. 2C. This difference map displays a strong positive density around the location of β2, indicating additional density due to binding of b_{sol} to this particular β subunit.

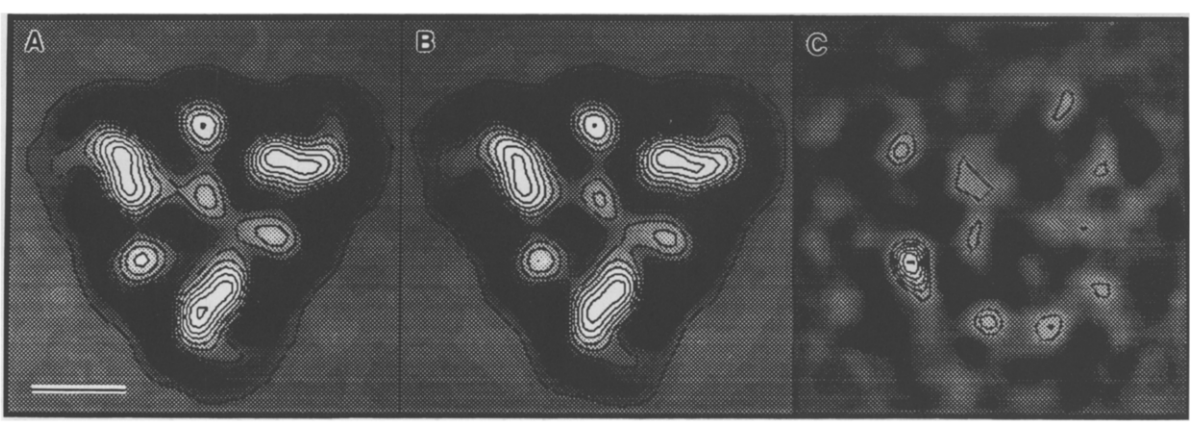

Fig. 2. (A) Total average of a dataset of 603 ECF_1 molecules, labeled with b_{sol} and anti-α Fab′ fragments. (B) Average of 366 molecules, labeled with anti-α Fab's only. Due to the inherent asymmetry of the $ECF_1(\alpha I\ Fab')_3$ complex, the three β subunits are distinguishable, with the top β (β1) being the strongest one, the bottom left β (β2) located next to the cavity and intermediate in density, and the bottom right β (β3) smeared out in density (see [9]). (C) Difference map generated by subtracting (B) from (A). Bar = 5 nm.

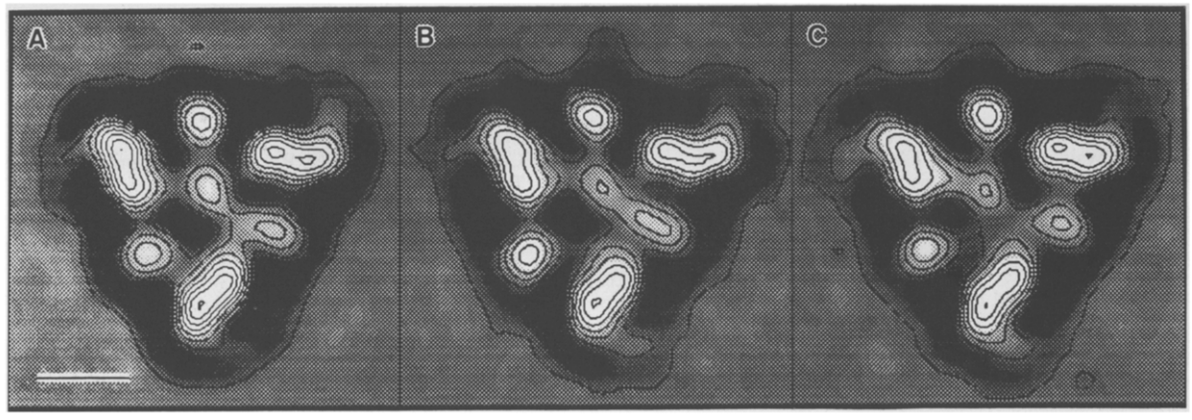

Fig. 3. The dataset of 603 b_{sol}-labeled molecules was treated by correspondence analysis and classification and sorted into three classes. The numbers of images averaged in A, B and C are 200, 165 and 238, respectively. Bar = 5 nm.

Due to the moderate binding affinity of b_{sol} for ECF_1 (see above) and the sample dilution necessary for cryoelectron microscopy (0.1 μM ECF_1), not all $ECF_1(\alpha I\ Fab')_3$ complexes in the data set are expected to have b_{sol} bound. The data set of the 603 single images was treated by correspondence analysis and classification and split arbitrarily into three classes, for which the averages are shown in Fig. 3A–C.

Only the average in Fig. 3B shows an increased density superimposed to $\beta 2$, which is obvious in this case due to sorting of the images. This class of images represent 27% of the data set, which is in good agreement with the expected number of images (32%), calculated for a 5-fold molar excess of b_{sol} dimer over 0.1 μM ECF_1 by assuming a binding constant for b_{sol} dimer of 1 μM [6]. The other two classes of images in Fig. 3A represent classes in which the central mass is differently located within the $\alpha_3\beta_3$ hexagon [9].

In the images shown in Fig. 3, the internal cavity is clearly located next to $\beta 2$. This cavity is not filled by binding of b_{sol} in the molecules contributing to the image average shown in Fig. 3B.

4. Discussion

Side views of the intact ECF_1F_0 observed in cryoelectron microscopy show the ECF_1 part attached to the membrane-intercalated F_0 part by a narrow stalk of about 45 Å in length [4], which is now thought to be composed of parts of the γ, δ and ε subunits of ECF_1 and the b subunit of F_0 [14]. A recent 6.5 Å resolution X-ray structure of mitochondrial F_1-ATPase

SUBUNIT

```
          82                                          100
ε         T A I R G Q D L D E A R A M E A K R K
                |   |   | | | |   |   | |
b         N K R R S Q I L D E A K A * E A E Q E
          79                                          96

         107                                          127
ε         S S H G D V D Y A Q A S A * * E L A K A I A Q
              |   |   |   |   | | |       |   | |   |
b         R A H K D L D L A K A S A T D Q L K K A E A E
          48                                          70
```

Fig. 4. Sequence homology between the b and ε subunits according to [16].

(MF_1) also shows an approximately 40 Å stalk representing the contribution of the F_1 subunits to the overall linkage between F_1 and F_0 parts [5].

In the hexagonal view of ECF_1, a cavity is observed within the ring of α and β subunits which is, in part, filled with segments of the γ subunit [7,9]. A similar cavity or pit is seen in the X-ray structure of MF_1 [5].

Cross-linking studies of ECF_1F_0 have provided evidence of the interaction of the b subunit dimer with both α and β subunits of the ECF_1 part [15]. This could occur by intercalation of a part of the b subunit dimer into the cavity within the F_1, or by association at the bottom of the complex without insertion into the cavity. The results presented here indicate that the second possibility is most likely. The density of b_{sol} is seen to superimpose on a β subunit when the ECF_1–b_{sol} complex is viewed in hexagonal projection with none of the additional density due to this approx. 31 kDa protein evident in the cavity.

Importantly, the interaction of the b_{sol} dimer is with a different β subunit ($\beta 2$) than the one which interacts with the ε subunit, i.e. $\beta 1$ (see [9]). It is interesting to note, therefore, the sequence homology first pointed out by Walker and co-workers [16] between the ε and the b subunit involving residues 82–100 and 107–127 in the ε subunit and residues 79–96 and 48–70 in the b subunit as shown in Fig. 4. In the ε subunit, this sequence includes Ser-108, which is involved in the binding to the C-terminal part of subunit $\beta 1$ [17].

Preliminary studies indicate that b_{sol} also interacts with the C-terminal part of a β subunit ($\beta 2$) (Dunn, S., unpublished observation), and we speculate that this is through the homologous sequence of the b subunit.

The fact that the b subunit does not extend into the cavity within the F_1 part leaves sufficient space for the extensive movements of the γ and ε subunits between catalytic sites that have been observed in cryoelectron microscopy studies [9,18].

Acknowledgements: Part of this work was supported by Grant MT-10237 from Medical Research Council of Canada to S.D., and National Institute of Health Grant HL 22456 to R.A.C.

References

[1] Senior, A.E. (1988) Physiol. Rev. 68, 177–231.
[2] Futai, M., Noumi, T. and Maeda, M. (1989) Annu. Rev. Biochem. 58, 111–136.

[3] Fillingame, R. (1990) The Bacteria: Bacterial Energetics, vol. XII (Krulwich, T.A., ed.) pp. 345–391, Academic Press, New York.
[4] Gogol, E.P., Lücken, U. and Capaldi, R.A. (1987) FEBS Lett. 219, 274–278.
[5] Abrahams, J.P., Lutter, R., Todd, R.J., vanRaaij, M.J., Leslie, A.G.W. and Walker, J.E. (1993) EMBO J. 12, 1775–1780.
[6] Dunn, S.D. (1992) J. Biol. Chem. 267, 7630–7636.
[7] Gogol, E.P., Aggeler, R.J., Sagermann, M. and Capaldi, R.A. (1989) Biochemistry 28, 4717–4724.
[8] Lücken, U., Gogol, E.P. and Capaldi, R.A. (1990) Biochemistry 29, 5339–5343.
[9] Wilkens, S. and Capaldi, R.A. (1994) Biol. Chem. Hoppe-Seyler 375, 43–51.
[10] Wise, J.G., Latchney, L.R. and Senior, A.E. (1981) J. Biol. Chem. 252, 3480–3485.
[11] Gogol, E.P., Lücken, U., Bork, T. and Capaldi, R.A. (1989) Biochemistry 28, 4709–4716.
[12] Aggeler, R.J., Mendel-Hartvig, J. and Capaldi, R.A. (1990) Biochemistry 29, 10387–10393.
[13] Frank, J., Shimkin, B. and Dowse, H. (1981) Ultramicroscopy 6, 343–358.
[14] Capaldi, R.A., Aggeler, R.J., Turina, P. and Wilkens, S. (1994) Trends Biochem. Sci. 19, 284–289.
[15] Aris, J.P. and Simoni, R.D. (1983) J. Biol. Chem. 258, 14599–14609.
[16] Walker, J.E., Gay, N.J., Saraste, M. and Eberle, A.N. (1984) Biochem. J. 224, 799–815.
[17] Dallmann, H.G., Flynn, T.G. and Dunn, S.D. (1992) J. Biol. Chem. 267, 18953–18960.
[18] Gogol, E.P., Johnston, E., Aggeler, R.J. and Capaldi, R.A. (1990) Proc. Natl. Acad. Sci. USA 87, 9585–9589.